Nuclear Instruments and Methods in Physics Research A 775 (2015) 71–76

Contents lists available at ScienceDirect

Nuclear Instruments and Methods in Physics Research A

journal homepage: www.elsevier.com/locate/nima

Digital pulse-timing technique for the neutron detector array NEDA

V. Modamio [a,*], J.J. Valiente-Dobón [a], G. Jaworski [b,c], T. Hüyük [d], A. Triossi [a], J. Egea [d,e], A. Di Nitto [f], P.-A. Söderström [g], J. Agramunt Ros [d], G. de Angelis [a], G. de France [h], M.N. Erduran [i], S. Ertürk [j], A. Gadea [d], V. González [e], J. Kownacki [c], M. Moszynski [k], J. Nyberg [l], M. Palacz [c], E. Sanchis [e], R. Wadsworth [m]

[a] Istituto Nazionale di Fisica Nucleare, Laboratori Nazionali di Legnaro, I-35020 Legnaro, Italy
[b] Faculty of Physics, Warsaw University of Technology, 00-662 Warszawa, Poland
[c] Heavy Ion Laboratory, University of Warsaw, 02-093 Warszawa, Poland
[d] Instituto de Física Corpuscular, CSIC-Universitat de València, E-46980 Valencia, Spain
[e] Department of Electronic Engineering, Universitat de València, E-46100 Burjassot, Spain
[f] Johannes Gutenberg-Universität Mainz, D-55099 Mainz, Germany
[g] RIKEN Nishina Center, 2-1 Hirosawa, Wako-shi, 351-0198 Saitama, Japan
[h] GANIL, CEA/DSAM and CNRS/IN2P3, F-14076 Caen, France
[i] Faculty of Engineering and Natural Sciences, Istanbul Sabahattin Zaim University, 34303 Istanbul, Turkey
[j] Nigde Universitesi, Fen-Edebiyat Falkültesi, Fizik Bölümü, 51240 Nigde, Turkey
[k] National Centre for Nuclear Research, 05-400 Otwock-Świerk, Poland
[l] Department of Physics and Astronomy, Uppsala University, SE-75120 Uppsala, Sweden
[m] Department of Physics, University of York, Heslington, YO1 5DD York, United Kingdom

ARTICLE INFO

Article history:
Received 5 June 2014
Received in revised form
19 September 2014
Accepted 1 December 2014
Available online 9 December 2014

Keywords:
Digital timing
Constant fraction discriminator
Liquid scintillator
BC501A
Neutron detector
NEDA

ABSTRACT

A new digital pulse-timing algorithm, to be used with the future neutron detector array NEDA, has been developed and tested. The time resolution of four 5 in. diameter photomultiplier tubes (XP4512, R4144, R11833-100, and ET9390-kb), coupled to a cylindrical 5 in. by 5 in. BC501A liquid scintillator detector was measured by employing digital sampling electronics and a constant fraction discriminator (CFD) algorithm. The zero crossing of the CFD algorithm was obtained with a cubic spline interpolation, which was continuous up to the second derivative. The performance of the algorithm was studied at sampling rates of 500 MS/s and 200 MS/s. The time resolution obtained with the digital electronics was compared to the values acquired with a standard analog CFD. The result of this comparison shows that the time resolution from the analog and the digital measurements at 500 MS/s and at 200 MS/s are within 15% for all the tested photomultiplier tubes.

1. Introduction

Neutron-detector arrays like the Neutron Wall [1,2] and the Neutron Shell [3] are being successfully used to identify very weak reaction channels in fusion-evaporation reactions in which exotic nuclei are produced after the emission of a few evaporated neutrons. These detector arrays are mainly used to determine the neutron multiplicity and require large detection efficiencies and good neutron-γ discrimination capabilities [4]. The organic liquid scintillator BC501A, with pulse-shape discrimination capabilities, is typically used in the aforementioned detector arrays. For the neutron detector array (NEDA), which presently is being developed, a detailed study of the dimensions and the type of liquid scintillator to use for the detector units has been published in Ref. [5]. In that paper, it was established that for optimal neutron efficiency the detector units should have a depth of 20 cm and a diameter of 5 in. and that they should be filled with a organic liquid scintillator BC501A. The light collection in this type of large cylindrical scintillators has been studied in detail [6], showing that the time resolution depends on the detector size of the liquid scintillators [4,7]. In addition, the size also dramatically changes the neutron-γ discrimination capabilities [4]. The uncertainty in the length of the neutron flight path, due to the large dimensions of the detectors in these arrays, does not allow an accurate measurement of the neutron energy using the time-of-flight methods. However, the use of fast photomultipliers for good timing accuracy is necessary in order to disentangle the fast and slow decay components for the pulse-shape analysis (PSA) to discriminate neutrons and γ-rays, as well as to measure the time-of-flight between adjacent detectors to identify scattered neutrons from two or more real neutron events [2,8]. The full NEDA array has been

* Corresponding author.
E-mail address: victor.modamio@lnl.infn.it (V. Modamio).

http://dx.doi.org/10.1016/j.nima.2014.12.002
0168-9002/

designed to efficiently identify reaction channels with one or more neutrons emitted from scattered events [5,9,10]. Its complete design comprises more than 300 detectors, covering a solid angle close to 2π and containing more than 1200 L of BC501A organic liquid scintillator [9]. The large number of channels in NEDA and the need of compatibility with other arrays, such as AGATA [11] and GALILEO [12] demands digital sampling electronics as a convenient replacement of the modular analog NIM electronics used in medium-scale nuclear physics experiments. Therefore, the NEDA array has been conceived to use digital electronics with a sufficiently high sampling rate to enable good timing and neutron-γ discrimination performance. For this purpose, a digitizer with 14 bits (11.7 effective number of bits, ENOB) and a sampling rate of 200 MS/s has been designed [13]. At the present time it has not been convincingly demonstrated that low sampling frequency digital modules are competitive with their analog predecessors for fast photomultipliers tubes (PMT). Therefore, one has to carefully check how the sampling rate and bandwidth constrain the digital timing performance compared to that obtained with analog electronics. For example, for very fast timing applications, it has been shown that digital algorithms for BaF_2 scintillators, using a 1 GS/s sampling ADC, can give a timing performance that is better than that obtained with traditional analog systems [14]. Besides achieving the best possible timing resolution, digital systems have been widely employed for PSA to perform neutron-γ discrimination with organic scintillators [15], using the zero-crossing [16] and double integration methods [17,18]. Specifically for the BC501A scintillator, digital neutron-γ discrimination has been widely exploited [19–22] and it has been shown that for PSA purposes a digitizer with a sampling rate of 200 MS/s and a resolution of 14 bits is suitable [20]. The present work aims to study the pulse-timing performance of four 5 in. PMTs (XP4512, ET9390-kb, R4144 and R11833-100) coupled to a 5 in. by 5 in. BC501A scintillator detector.

In order to quantify the timing properties of the PMTs, a CFD algorithm was developed. The zero-crossing of the CFD was obtained with a cubic spline interpolation, which was continuous up to the second derivative. The waveforms were digitized with a 12-bit resolution 500 MS/s fast-ADC and were downsampled to 200 MS/s in order to mimic the future electronics of the NEDA array. The performance of the algorithm, with respect to the timing resolution, was studied at the sampling rates 500 and 200 MS/s and compared to results obtained with a standard analog CFD.

2. Experimental setup and measurements

A schematic picture of the experimental setup is shown in Fig. 1. γ-rays from a ^{60}Co source were measured in coincidence between a cylindrical 5 in. by 5 in. BC501A liquid scintillator detector and a cylindrical 1 in. by 1 in. BaF_2 crystal. The distance from the source to the front face of the detectors was 20 cm and 5 cm for the BC501A and BaF_2 detectors, respectively. The detectors were placed at an angle of 90° with respect to the outgoing γ-rays. A 5 cm thick lead shield was placed between the detectors in order to minimize the detection of γ-rays that were scattered from one detector into the other. The lead brick did not shadow the detectors from the ^{60}Co source.

The tested 5 in. PMTs were Photonis XP4512, Hamamatsu R4144, Hamamatsu R11833-100 and ET Enterprises ET9390-kb, which in turn were coupled to the same liquid scintillator detector. The BaF_2 crystal was coupled to a fast 2 in. PMT of model Hamamatsu R2059. All PMTs were magnetically shielded with μ-metal. The high voltage (HV) of all tested PMTs was set to get an anode signal amplitude of 1 V/MeV, while the HV for the BaF_2 PMT was set to −1806 V. Table 1 shows the HV values used for the 5 in. PMTs.

The anode signals from the detectors were connected to LeCroy N428A linear fan-in/fan-out units, from which the output signals were

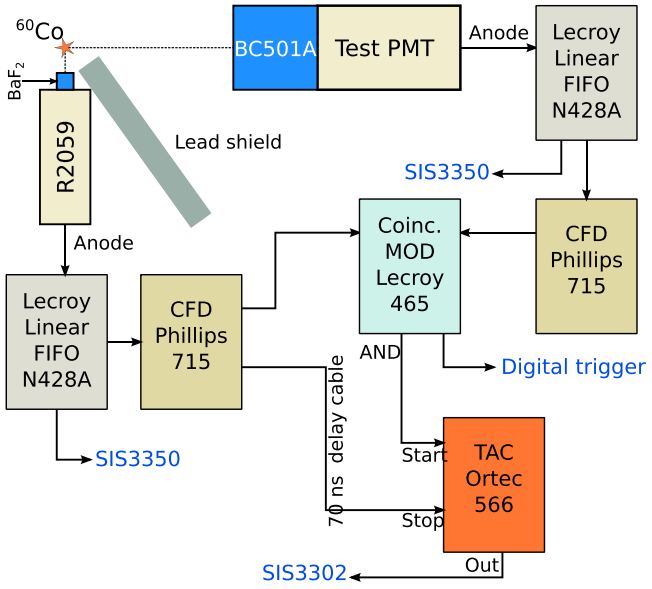

Fig. 1. Schematic picture of the setup employed for the pulse-timing measurements. The analog and digital electronics chains are indicated. A lead shield (grey block) is place in between the detectors in order to avoid scattered gammas from one detector to the other.

Table 1
High voltage (HV) settings for the PMTs, threshold (Th) and shaping delay (Δ) values used by the analog CFD.

Detector	HV (V)	Th (mV)	Δ (ns)
R2059 (BaF_2)	−1806	−40(5)	5
XP4512	−1140	−35(5)	10
R4144	−1452	−40(5)	10
R11833-100	−1390	−40(5)	12
ET9390-kb	−1206	−30(5)	25

sent to the sampling ADCs and to analog CFD units of type Phillips 715. The values of the thresholds and shaping delays of the CFD for the 5 in. PMTs are given in Table 1. The thresholds were adjusted to the minimum and the shaping delays were optimised to obtain the best possible time resolution. For the BaF_2 detector, the CFD threshold was set to −40 mV and the shaping delay to 5 ns. All detectors were running with count rates of 4 kHz, with a coincidence rate of about 30 Hz. The analog time difference between the BC501A and BaF_2 detectors was obtained by using an Ortec 566 TAC (500 ns range). The start and stop signals of the TAC were the CFD signals from the BC501A and BaF_2 detectors, respectively. For the stop signal, a delay of 70 ns was used. The start signal was only produced if it overlapped in time with a wide BaF_2 signal in the coincidence unit LeCroy 465. A signal from this unit was also used as a trigger for the data acquisition system. The detector waveforms were digitized with a sampling ADC of model Struck SIS3350, a VME unit with four channels, each with a sampling frequency of 500 MS/s, a resolution of 12 bits (9.2 ENOB) and a dynamic range of 2 V. The analog output signal from the TAC was digitized with a Struck SIS3302 sampling ADC (single width 6U VME, 8 channels, 100 MS/s, 16 bit). The digitizers were read out through the VME bus and the data were sent to the data acquisition system via a Struck SIS3100 controller using an optical link. The pulse-timing properties of the 5 in. PMTs were studied at the sampling rates 500 MS/s and 200 MS/s. The original waveforms, sampled at 500 MS/s were downsampled to 200 MS/s, using as a filter a discrete averaging with an effective cutoff frequency at 100 MS/s. The signal from the BaF_2 detector was always sampled at 500 MS/s.

3. Results and discussion

In this section, the time resolution obtained with the digital method will be discussed and compared with the results from the analog measurements. Fig. 2 shows the waveforms digitized at 500 MS/s for the four tested PMTs, averaged over 100k signals. The risetimes (10–90%) extracted from the average waveforms were 4.9(4) ns, 3.8(3) ns, 6.3(7) ns and 13.5(13) ns for the PMTs XP4512, R4144, R11833-100 and ET9390-kb, respectively. Uncertainties given correspond to 1σ. At 500 MS/s, the fastest PMTs provide only 2 or 3 sampling points on the rising edge of the signal. Thus, accurate timing algorithms should rather use sampling points from a range that is larger than the rising edge of the signal. Fig. 3 shows the risetime extracted from the digitized waveforms as a function of the signal amplitude. As seen in the figure, there is no appreciable dependence of the risetime on the signal amplitude for any of the PMTs, which shows that the constant fraction is a suitable technique for these signals. Digital constant fraction algorithms have already been studied in different systems, such as 100 MS/s sampled waveforms from charge sensitive preamplifiers [23], or for signals from BaF_2 scintillators [14]. Such algorithm has also been implemented digitally on FPGA devices employing a linear interpolation of the zero crossing [24]. However, the cubic spline interpolation for pulse timing has been shown to improve the resolution considerably in certain systems [23]. Consequently, a constant fraction algorithm was developed in this work with the zero-crossing time determined using a cubic spline interpolation, with continuous first and second derivatives. A zero-crossing signal ZC_i is created by summing the original waveform S_i multiplied by a factor χ and its inverted signal delayed by an integer number of samples Δ:

$$ZC_i = \chi(S_i - BS) - (S_{i-\Delta} - BS). \quad (1)$$

The baseline BS is first calculated as an average of the first 50 samples and then subtracted from both the delayed and scaled components. The zero-crossing point is then obtained by interpolating between the

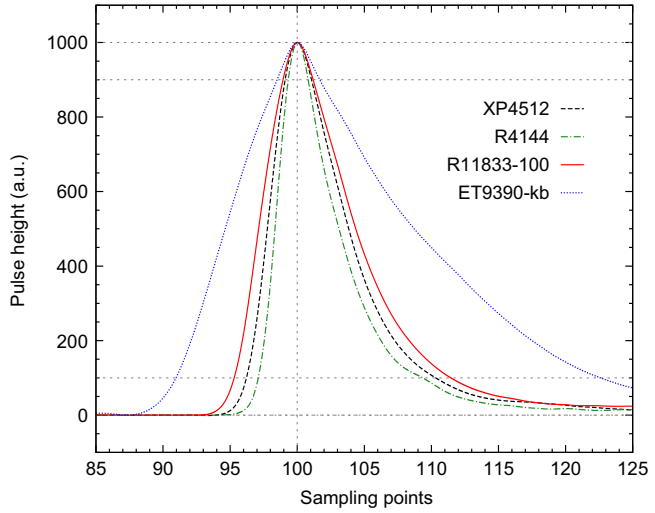

Fig. 2. Digitized waveforms averaged over 10^5 events for the four 5 in. PMTs coupled to a cylindrical 5 in. by 5 in. BC501A. The sampling frequency of the digitizer was 500 MS/s. The waveforms were normalized to a pulse height of 1000 and time aligned at the maximum of the signal. Dashed lines are drawn at 10%, 90%, at the maximum and at the baseline of the waveform to guide the eye.

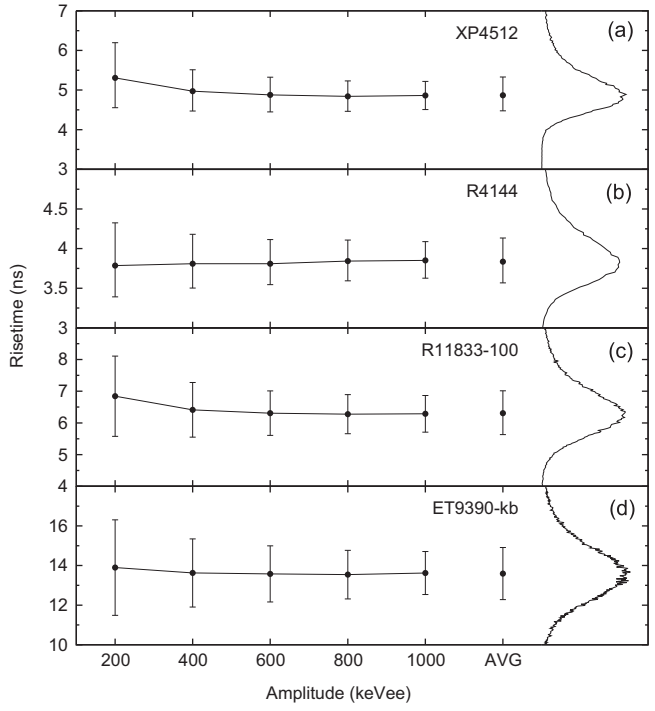

Fig. 3. Risetime as a function of the signal amplitude determined from the digitized waveforms for the PMTs (a) XP4512, (b) R4144, (c) R11833-100 and (d) ET9390-kb. The width of the amplitude windows were 100 keVee. The values obtained for all amplitudes above a threshold of 100 keVee are shown at the x axis position labeled AVG and the risetime distributions for this case are plotted on the right hand side. Error bars indicate the 2σ width of the risetime distributions.

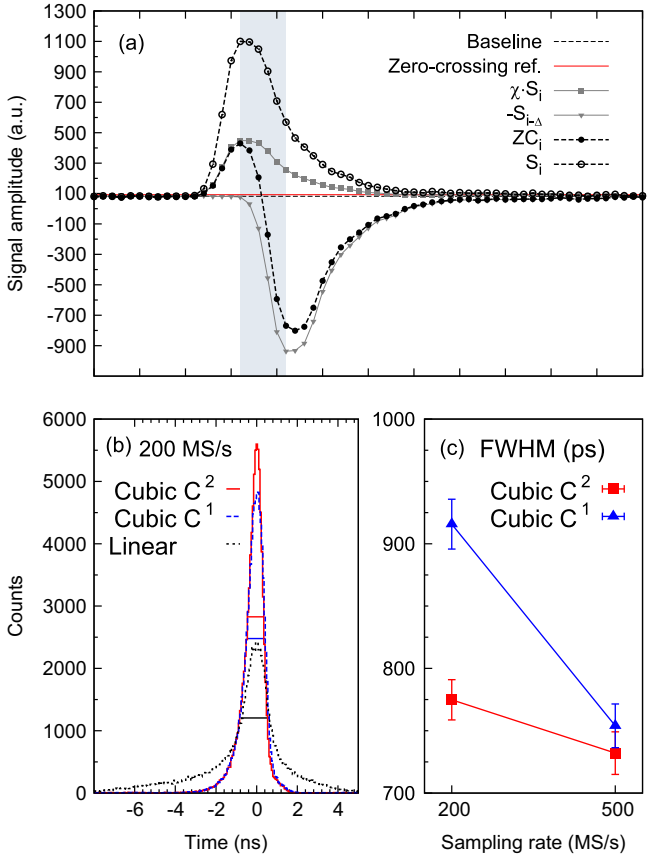

Fig. 4. Illustration of the digital constant fraction algorithm. (a) An example of a waveform and its zero-crossing signal, measured with the R11833-100 PMT at a sampling rate of 500 MS/s. The horizontal black dash line is the baseline and the horizontal solid red line is the reference to get the zero-crossing. The grey area indicates the samples used for the cubic interpolation C^2. (b) Time-difference distribution obtained with the R11833-100 PMT at 200 MS/s using the linear, cubic C^1 and cubic C^2 interpolations. (c) Time resolution as a function of sampling frequency for the R11833-100 PMT using cubic C^1 and C^2 interpolations. (For interpretation of the references to colour in this figure caption, the reader is referred to the web version of this paper.)

first negative sample and the preceding sample, at a reference height of 5 mV over the baseline. The interpolation consists of a cubic spline employing 6 sampling points, with continuous first and second derivatives (C^2). The delay Δ, together with the factor χ were chosen in order to optimize the time resolution of each PMT. With this two-parameter digital method, the best timing result was obtained for all PMTs by using a slightly shorter delay compared to the shaping delay used with the analog CFD module. Fig. 4a shows an example of the waveform S_i, the scaled signal $\chi \cdot S_i$, the delayed and inverted signal $-S_{i-\Delta}$, and the resulting zero-crossing signal ZC_i measured with the PMT R11833-100. The grey area highlights the six sampling points used for the zero-crossing interpolation. It contains all the samples in the leading edge of the delayed and inverted signal. The cubic spline interpolation C^2 was compared with a cubic spline interpolation C^1 (continuous only up to the first derivative), in which four points were employed, and with a linear interpolation. Fig. 4b shows as an example the time distribution obtained for the PMT R11833-100 with the three different interpolations at a sampling rate of 200 MS/s and with a threshold of 100 keVee. The use of a cubic spline interpolation improved significantly the time resolution with respect to the linear one: the FWHM was 1460(120) ps with the linear interpolation, 920 (20) ps with the cubic spline interpolation C^1 and 760(20) ps with the cubic spline interpolation C^2. Additionally, the cubic spline interpolation significantly reduces the tailing of the distribution with respect to the linear interpolation. The use of six sampling points and a C^2 cubic function, led to much better results when the sampling rate was lowered. Fig. 4c shows the time resolution for the cubic interpolations at the sampling rates 500 MS/s and 200 MS/s for the PMT R11833-100. While both algorithms achieve the same time resolution at 500 MS/s, the C^2 cubic spline interpolation improves the time resolution by 15% compared to the C^1 interpolation at 200 Ms/s. The time resolution of all four PMTs, using both analog and digital electronics, was evaluated from time distributions containing 10^5 events. One additional measurement was performed by using two XP4512 PMTs and two cylindrical 5 in. by 5 in. BC501A detectors. This was done in order to estimate the contribution of the BaF_2 reference detector to the evaluated time resolution. The result obtained was that the FWHM of the BaF_2 detector was at most 200 ps.

Fig. 5 shows the time resolution as a function of signal amplitude in keVee for the four tested PMTs and measured with both analog and digital electronics at the sampling rates 500 MS/s and 200 MS/s. For all measurements, the time resolution achieved with the digital system at 500 MS/s was at least as good as the ones obtained with the analog electronics. For signals with large amplitudes, the time resolution of the digital system at 500 MS/s was better than the analog one for the XP4512 and R4144 PMTs.

It may be noticed that the intrinsic time resolution of the analog and digital modules is considered similar, and negligible with respect

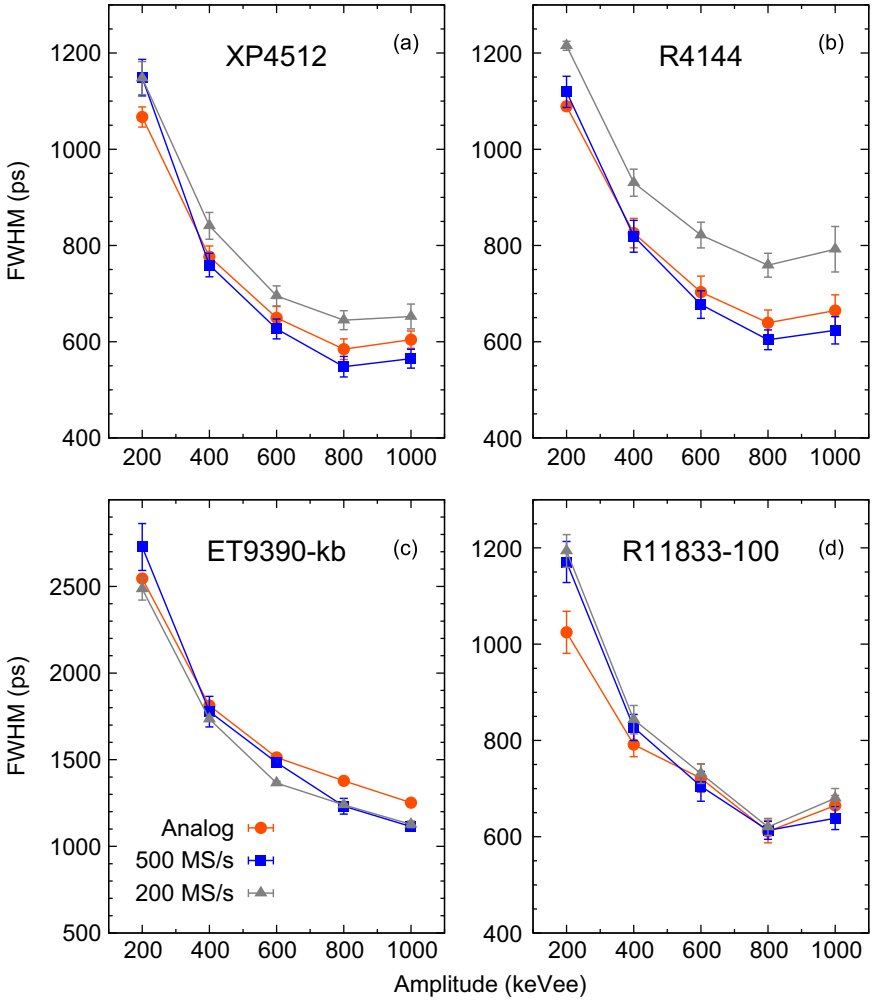

Fig. 5. Time resolution FWHM for (a) XP4512, (b) R4144, (c) ET9390-kb and (d) R11833-100 PMTs as a function of the waveform amplitude, for 500 MS/s (blue squares), 200 MS/s (grey triangles) and analog result (red circles). Amplitude slices are 100 keVee width. (For interpretation of the references to colour in this figure caption, the reader is referred to the web version of this paper.)

to the nanosecond range of the time resolution for the whole system. For example, the time resolution of a pulser digitized with a 250 MS/s flash ADC is ~60 ps [25], a value which is similar to the time walk of commercial analog CFD modules. A summary of the time resolution obtained with the analog and digital systems at a threshold of 100 keVee, is shown in Table 2. The table also includes the measured average risetimes, the blue sensitivity and the measured number of photoelectrons per MeV of the PMTs. For all measurements, the FWHM refers to the total resolution of the system, including the contribution from the BaF_2 reference detector. The timing performance obtained in the present work is compared with that of the neutron detector array DEMON [26]. Those detectors are large BC501A liquid scintillators, 16 cm diameter and 20 cm depth. Table 3 shows the results of the timing measurements with the XP4512 and R4144 PMTs obtained in this work with the results reported in Ref. [26] for the DEMON detectors. Since both tests were done with different samples of PMTs and different sizes of the liquid scintillator detectors, a comparison of the results from both experiments was done by normalising the time resolution to the mean number of photoelectrons in the Compton distribution of the γ-rays from ^{60}Co with a 100 keVee energy threshold, that is FWHM $\cdot \sqrt{N_{phe}}$. The poorer time resolution of the DEMON detectors is due to the larger size of the scintillator. However, the small difference in the time resolution, normalized as FWHM $\cdot \sqrt{N_{phe}}$, indicates that both experiments achieve the same timing performance for the PMTs XP4512 and R4144.

The digital performance of each PMT is correlated with the signal risetime and the number of photoelectrons. On one hand, the PMTs XP4512, R4144 and R11833-100, with risetimes 4.9(4), 3.8(3) and 6.3(7) ns, respectively, achieve a similar average time resolution of better than FWHM = 750 ps with analog electronics. The worse time resolution for the ET9390-kb, with a FWHM of 1470 ps, is due to its significantly larger signal risetime of 13.5(13) ns. On the other hand, the time resolution strongly depends on the number of photoelectrons N_{phe} emitted from the photocathode. This is translated to a dependency of energy as $1/\sqrt{E}$ [27], making also the PMT blue photocathode sensitivity S_{pc} an important parameter for the time resolution. The R11833-100 and ET9390-kb PMTs are slower, but have higher S_{pc} values, than the other two PMTs (see Table 2). Therefore they exhibit less degradation in time resolution when downsampling from 500 MS/s to 200 MS/s. The increase of the FWHM values at the very end of the Compton edge (above 800 keV, see Fig. 5) is worth noticing. This is interpreted as being due to multiple-Compton scattering of γ rays inside the detector. In such cases, the production of light at two (or more) locations inside the scintillator worsens the time resolution.

Table 2
Measured risetime, blue photocathode sensitivity S_{pc}, number of photoelectrons N_{phe}, and time resolution *FWHM* for the tested PMTs, with the R2059/BaF_2 as reference. An energy cutoff of 100 keVee was applied. The blue sensitivity is taken from the manufacturer data, measured with Corning blue filter CS 5-58 polished to the half stock thickness.

PMT	Risetime (ns)	S_{pc} (μA/lm)	N_{phe} (MeV^{-1})	Analog	Time resolution FWHM (ps)	
					500 MS/s	200 MS/s
XP4512	4.9(4)	10.6	1330(70)	690(30)	660(30)	740(30)
R4144	3.8(3)	10.2	950(60)	750(30)	710(30)	870(30)
R11833-100	6.3(7)	13.5	1830(90)	743(13)	730(20)	760(20)
ET9390-kb	13.5(13)	12.0	1550(50)	1470(20)	1330(30)	1360(20)

Table 3
Comparison of the PMT tests performed in the present experiment (NEDA) with the results obtained for the DEMON arrangement.

PMT Setup	N_{phe} (MeV^{-1})	N_{phe} ^{60}Co[a] (MeV^{-1})	FWHM (ps)	FWHM $\cdot\sqrt{N_{phe}}$ (ps $\cdot$ MeV$^{-1/2}$)
XP4512				
NEDA	1330(70)	732(42)	690(30)	$1.87(10)\times10^4$
DEMON[b]	1070(55)	590(30)	890(40)	$2.16(11)\times10^4$
R4144				
NEDA	950(60)	523(36)	750(30)	$1.72(9)\times10^4$
DEMON[b]	900(45)	495(25)	850(40)	$1.89(10)\times10^4$

[a] Mean photoelectron number in the Compton distribution of ^{60}Coγ-rays above 100 keV energy threshold.
[b] Test with a BC501A scintillator of the DEMON detector, 16 cm diameter and 20 cm length. See Ref. [26].

4. Conclusions

In summary, the timing performance of four 5 in. PMTs (XP4512, R4144, R11833-100, ET9390-kb), connected to a cylindrical 5 in. by 5 in. BC501A scintillator detector, were measured by using digital electronics and a fast BaF_2 detector as time reference. The detector waveforms were digitized by a flash ADC with a resolution of 12 bits and sampling frequency of 500 MS/s. Measurements were also performed with the sampling frequency downsampled to 200 MS/s. A CFD algorithm, consisting of a zero-crossing signal obtained as a cubic spline interpolation continuous up to the second derivative, was applied on the digitized waveforms. The obtained time resolution was compared to the results obtained with a standard analog CFD. Similar time resolution was achieved with the analog measurement and the digital measurement at 500 MS/s, with only a small degradation at 200 MS/s. Among the four different PMTs tested, the XP4512 and R11833-100 PMTs performed slightly better at 200 MS/s compared to the other models, giving a FWHM value that was lower than 800 ps. From the present digital measurements, one can state that the use of a digitizer with a sampling rate of 200 MS/s and a resolution of 12 bits will give a time resolution for the detectors of the future NEDA array that is as good as what can be obtained with a standard analog CFD.

Acknowledgements

Work partially supported by the Generalitat Valenciana, Spain, under grant PROMETEO/2010/101 and PROMETEO/2014/019, by MINECO, Spain, under grants AIC-D-2011-0746, FPA2011-29854 and FPA2012-33560, by the STFC, UK and by the Swedish Research Council.

References

[1] Ö. Skeppstedt, H. Roth, L. Lindström, R. Wadsworth, I. Hibbert, N. Kelsall, D. Jenkins, H. Grawe, M. Gorska, M. Moszyński, et al., Nuclear Instruments and Methods in Physics Research Section A: Accelerators, Spectrometers, Detectors and Associated Equipment 421 (3) (1999) 531.
[2] J. Ljungvall, M. Palacz, J. Nyberg, Nuclear Instruments and Methods in Physics Research Section A: Accelerators, Spectrometers, Detectors and Associated Equipment 528 (3) (2004) 741.
[3] D. Sarantites, W. Reviol, C. Chiara, R. Charity, L. Sobotka, M. Devlin, M. Furlotti, O. Pechenaya, J. Elson, P. Hausladen, et al., Nuclear Instruments and Methods in Physics Research Section A: Accelerators, Spectrometers, Detectors and Associated Equipment 530 (3) (2004) 473.
[4] M. Moszyński, G. Costa, G. Guillaume, B. Heusch, A. Huck, S. Mouatassim, Nuclear Instruments and Methods in Physics Research Section A: Accelerators, Spectrometers, Detectors and Associated Equipment 350 (1) (1994) 226.
[5] G. Jaworski, M. Palacz, J. Nyberg, G. De Angelis, G. De France, A. Di Nitto, J. Egea, M. Erduran, S. Ertürk, E. Farnea, et al., Nuclear Instruments and Methods in Physics Research Section A: Accelerators, Spectrometers, Detectors and Associated Equipment 673 (2012) 64.
[6] M. Moszyński, Study of light collection process from cylindrical scintillators, Nuclear Instruments and Methods 134 (1) (1976) 77.
[7] K. Banerjee, T. Ghosh, S. Kundu, T. Rana, C. Bhattacharya, J. Meena, G. Mukherjee, P. Mali, D. Gupta, S. Mukhopadhyay, et al., Nuclear Instruments and Methods in

Physics Research Section A: Accelerators, Spectrometers, Detectors and Associated Equipment 608 (3) (2009) 440.
[8] J. Cederkäll, B. Cederwall, A. Johnson, M. Palacz, Nuclear Instruments and Methods in Physics Research Section A: Accelerators, Spectrometers, Detectors and Associated Equipment 385 (1) (1997) 166.
[9] T. Hüyük, et al., Monte carlo simulations for the different configurations of NEDA array, LNL Annual report 2011 (2011) 62.
[10] A. Pipidis, et al., The genesis of neda (neutron detector array): characterizing its prototypes, LNL Annual report 2010 (2010) 78.
[11] S. Akkoyun, A. Algora, B. Alikhani, F. Ameil, G. De Angelis, L. Arnold, A. Astier, A. Ataç, Y. Aubert, C. Aufranc, et al., Nuclear Instruments and Methods in Physics Research Section A: Accelerators, Spectrometers, Detectors and Associated Equipment 668 (2011) 26.
[12] D. Mengoni, et al., LNL Annual report 2013.
[13] X. Egea, E. Sanchis, V. Gonzalez, A. Gadea, J.M. Blasco, D. Barrientos, J. Valiente Dobon, M. Tripon, A. Boujrad, C. Houarner, et al., Design and test of a high-speed flash adc mezzanine card for high-resolution and timing performance in nuclear structure experiments, in: 18th IEEE-NPSS Real Time Conference (RT), 2012, IEEE, 2012, pp. 1–8.
[14] M.A. Nelson, B.D. Rooney, D.R. Dinwiddie, G.S. Brunson, Nuclear Instruments and Methods in Physics Research Section A: Accelerators, Spectrometers, Detectors and Associated Equipment 505 (1) (2003) 324.
[15] M. Flaska, M. Faisal, D.D. Wentzloff, S.A. Pozzi, Nuclear Instruments and Methods in Physics Research Section A: Accelerators, Spectrometers, Detectors and Associated Equipment 729 (2013) 456.
[16] M. Nakhostin, P. Walker, Nuclear Instruments and Methods in Physics Research Section A: Accelerators, Spectrometers, Detectors and Associated Equipment 621 (1) (2010) 498.
[17] M. Flaska, S.A. Pozzi, Nuclear Instruments and Methods in Physics Research Section A: Accelerators, Spectrometers, Detectors and Associated Equipment 599 (2) (2009) 221.
[18] Y. Kaschuck, B. Esposito, Nuclear Instruments and Methods in Physics Research Section A: Accelerators, Spectrometers, Detectors and Associated Equipment 551 (2) (2005) 420.
[19] M. Moszynski, G. Bizard, G. Costa, D. Durand, Y. El Masri, G. Guillaume, F. Hanappe, B. Heusch, A. Huck, J. Peter, et al., Nuclear Instruments and Methods in Physics Research Section A: Accelerators, Spectrometers, Detectors and Associated Equipment 317 (1) (1992) 262.
[20] P.-A. Söderström, J. Nyberg, R. Wolters, Nuclear Instruments and Methods in Physics Research Section A: Accelerators, Spectrometers, Detectors and Associated Equipment 594 (1) (2008) 79.
[21] E. Ronchi, P.-A. Söderström, J. Nyberg, E. Andersson Sundén, S. Conroy, G. Ericsson, C. Hellesen, M. Gatu Johnson, M. Weiszflog, Nuclear Instruments and Methods in Physics Research Section A: Accelerators, Spectrometers, Detectors and Associated Equipment 610 (2) (2009) 534.
[22] X.L. Luo, et al., Nuclear Instruments and Methods in Physics Research Section A: Accelerators, Spectrometers, Detectors and Associated Equipment 767 (2014) 83.
[23] L. Bardelli, G. Poggi, M. Bini, G. Pasquali, N. Taccetti, Nuclear Instruments and Methods in Physics Research Section A: Accelerators, Spectrometers, Detectors and Associated Equipment 521 (2) (2004) 480.
[24] A. Fallu-Labruyere, H. Tan, W. Hennig, W. Warburton, Nuclear Instruments and Methods in Physics Research Section A: Accelerators, Spectrometers, Detectors and Associated Equipment 579 (1) (2007) 247.
[25] J. Agramunt, Private Communication (2013).
[26] M. Moszyński, G. Costa, G. Guillaume, B. Heusch, A. Huck, S. Mouatassim, Nuclear Instruments and Methods in Physics Research Section A: Accelerators, Spectrometers, Detectors and Associated Equipment 307 (1) (1991) 97.
[27] B. Bengtson, M. Moszyński, Nuclear Instruments and Methods 81 (1) (1970) 109.